Journal Name

ARTICLE

The influence of oxygen vacancy and Ce^{3+} ion positions on the properties of small gold clusters supported on CeO_{2-X}(111)

Received 00th January 20xx,
Accepted 00th January 20xx

DOI: 10.1039/x0xx00000x

www.rsc.org/

Julien Engel,[a] Elise Schwartz,[b] C. Richard A. Catlow,[a] and Alberto Roldan[a]*

We studied the influence of oxygen vacancies on small Au clusters supported on CeO_2 using dispersion-corrected density functional theory (DFT-D). Our results show that the effect of oxygen vacancies on Au clusters is highly dependent on the cluster size and the relative position of the cluster to the vacancy. We found that the Au particles are only affected by the vacancies if they are located directly within the cluster perimeter. Using Crystal Orbital Hamilton Population (COHP) analysis, we show that the oxygen vacancy can lead to the formation of Au-Ce bonds under destabilisation of the bonds to the Au atom at the vacancy site and subsequent distortion of the cluster structure. However, we found that such Au-Ce bond formation only occurs when the interactions between the Au atom at the vacancy site and the surround Au atoms are not critical for the overall cluster stability as, for example, in the case of the central atom in a planar Au_7 cluster. The formation of an oxygen vacancy can change the charge of the supported gold cluster from positive (on stoichiometric CeO_2) to neutral or negative on defective CeO_{2-X}. Interestingly, the additional electron density is located only at the Au atom at the vacancy site and is not redistributed throughout the cluster. Investigation of the electrostatic potential of the cluster surface did not show any significant changes compared to the stoichiometric surface, which is not caused by structural changes of the Au cluster.

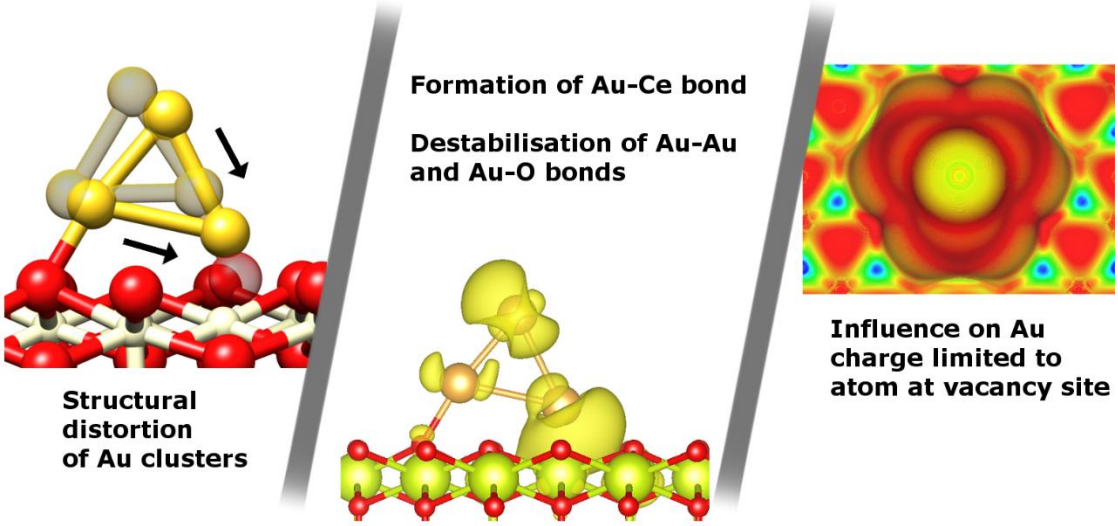

[a] School of Chemistry, Cardiff University, Main Building, Park Place, Cardiff, CF10 3AT, Wales, United Kingdom
[b] Hôtel Technologique, 45 Rue Frédéric Joliot Curie, 13382 Marseille Cedex 13

Electronic Supplementary Information (ESI) available: Structures of the supported Au clusters, DOS and COHP plots, electron density iso-surfaces, and electrostatic potential plots can be found in the Supporting Information. This material is available free of charge via the Internet at DOI: 10.1039/x0xx00000x. All data created during this research is openly available from the University of Cardiff Research Portal at DOI: 10.17035/d.2020.0098139066.

Introduction

Supported metal catalysts are used for a wide range of industrial chemical processes.[1–3] Gold clusters are of particular interest due to their activity and selectivity in many important reactions such as hydrochlorination,[4] low-temperature

oxidation of CO,[5,6] the water-gas shift reaction[7], and other organic reactions.[8] The activity of gold clusters is highly size dependent[9] and known to decrease above a particle size of 5 nm .[10,11] This effect has been attributed to various factors, such as a high surface-to-bulk ratio, the availability of low-coordination atoms,[12] and the presence of perimeter sites at the Au–support interface.[13]

The Au_n/CeO_{2-X} system has been the subject of several computational studies although most of them focussed on very small clusters.[14–18] Chutia et al.[27] studied single gold atoms and demonstrated that electron transfer to the gold occurred over vacancies. Zhang *et al.* investigated the structures and properties of Au clusters with up to 11 atoms, but all their structures were built under the precondition that one of the Au atoms is located at a vacancy site.[19] Teng *et al.* studied the structures and adsorption energies of a series of Au clusters in the range of 1-10 atoms and they conclude that the oxygen vacancy stabilises the Au clusters depending on the size of the cluster and the position of the vacancy.[20] Both, Zhang and Teng, did not explore the localisation of the Ce^{3+} ions.

The interface between the oxide surface and the nano-particle clearly influences the structural parameters of the supported particles such as shape and their electronic properties.[21–23] We recently performed a comparative study on the structural and electronic effects of different support materials, namely magnesium oxide (MgO), cerium (IV) oxide (CeO_2) and graphene (C), on small Au clusters with particular focus on the interface mismatch.[24] We limited that study to defect-free surfaces to reduce the complexity of the investigated systems. While the most stable surface of MgO, i.e. (001),[25] can be prepared relatively defect-free,[26] ceria (CeO_2) is highly reducible at low O_2 chemical potential leading to the formation of oxygen vacancies.[27] These defects can influence the properties of the supported clusters.[28] The present study, therefore, aims to understand in detail how the vacancies affect the Au_n particles. However, the introduction of vacancies into the Au_n/CeO_2 model is more challenging than it might seem at first since it is more complicated than merely removing oxygen atoms from the surface. First, the creation of such vacancies breaks the symmetry of the surface and dramatically increases the search space for the lowest energy structures since the position of the cluster relative to the vacancy becomes important. Second, previous studies have shown that the formation an oxygen vacancy in CeO_2(111) leads to the reduction of two Ce^{4+} ions to Ce^{3+}. Multiple minima for the localisation of the Ce^{3+} ions exist even in a naked defective surface with a single oxygen vacancy with tenths of electron volts difference in energy.[29] Since the environment of Ce ions is influenced by the presence of the Au_n cluster, the magnitude of the energy difference and the number of non-equivalent positions might increase. Both issues make this study a highly multidimensional problem and it becomes difficult to identify the lowest structural or electronic minimum in static quantum chemical calculations, especially with increasing system size. The combination of electronic structure calculations with genetic algorithms might be considered to explore comprehensively this system, but because of the interplay of geometry and Ce^{3+} ion localisation a very large number of configurations would need to be explored, making the computational expense prohibitive. The problem of vacancy cluster interactions is, however, highly relevant to any study on the reactivity of CeO_{2-X}-supported Au particles and key questions can be answered despite the difficulty in identifying global energy minima. They concern first, how cluster properties such as its geometry and charge distribution are affected by the introduction of an oxygen vacancy, which will influence the cluster's reactivity; and secondly, the influence of variations in oxygen vacancy positions and Ce^{3+} ion positions on cluster properties, which will guide future studies.

Computational Details

Spin-polarised periodic plane-wave density functional theory calculations were performed with the Vienna *Ab Initio* Simulation Package (VASP 5.4.4).[30–32] The density functional of Perdew, Burke, and Ernzerhoff (PBE)[33] was used to calculate the exchange and correlation contributions. To describe long-range interactions, which were shown to be necessary for Au_n clusters[34] and metal oxide surfaces,[35] Grimme's empirical dispersion correction DFT-D3 was used.[36] It was shown that PBE-D3 is in good agreement with the vdW-DF optB88 for the structure of Au clusters.[24] The projector-augmented wave (PAW) formalism[32,37] implemented in VASP was employed to describe the core electrons. A plane-wave kinetic cut-off was set at 500 eV. The Brillouin zone was sampled on a Monkhorst-Pack grid[38] with 7×7×1 k-points for the small surfaces and 3×3×1 k-points for the large surfaces, respectively (see below for details on the slab models). A Hubbard approach correction (DFT+U) using the method of Liechtenstein *et al.* was used on the Ce 4f-orbitals.[39–45] The parameters were set to U_{eff} = 4 eV (U = 5 eV and J = 1 eV), which better reproduce the reduction of CeO_2 as shown in our benchmarking calculations[24] and previous reports.[46,47] Dipole corrections were applied perpendicular to the surfaces upon adsorption of gold clusters. Bader charges were calculated to assign partial charges to specific atoms.[48] Crystal Orbital Hamilton Populations (COHP) were calculated with the Lobster 2.2.1 code.[49–52]

To determine the distance between the surface and the gold clusters, the surface height was defined as the average height of the top oxygen layer and the cluster height as the average height of all atoms within z ≤ 0.3 Å of the lowest gold atom. The average gold-gold distance within the metal clusters is calculated as the average of all neighbour distances. Two atoms are defined as neighbours if the distance between them is below twice the van-der-Waals radius (r_{vdW} = 1.66 Å).[53]

We calculated the adsorption energies (E_{ads}) from the total energy of the optimised structure of the gold cluster on the surface ($E_{Aun\text{-}S}$), the energy of the optimised naked slab (E_S), and the energy of the gold cluster in gas phase retaining the shape from the supported structure (E_{Aun}).

$$E_{ads} = \frac{E_{Aun-S} - (E_S + E_{Aun})}{n} \quad (Eq. 1)$$

The cohesion energy per atom (E_{coh}) of the Au clusters was calculated with equation 2 using the gas-phase energy of a single gold atom (E_{Au1}).

$$E_{coh} = \frac{E_{Aun} - n \cdot E_{Au1}}{n} \quad (Eq. 2)$$

The electrostatic potential was determined as implemented in VASP.[54] The energies reported here correspond to the energies of a particle with a charge of −e within the electrostatic potential V(r) (equation 3).

$$V(r) = \sum_A \frac{Z_A}{|R_A - r|} - \int \frac{\rho(r')dr'}{|r' - r|} \quad (Eq. 3)$$

Structures and iso-surfaces were visualised with the program *Visualisation for Electronic and Structural Analysis* (VESTA)[55] and CHIMERA[56], respectively.

Slab models

As in our previous study, two different slab models of the CeO_{2-X}(111) were used in this work.[24] A three-trilayered oxygen-terminated slab (3×3×3) with 27 Ce and 53 O atoms (surface area = 116.5 Å^2) was chosen for clusters with up to four Au atoms. Larger clusters were calculated on a two-trilayered surface (6×6×2; surface area = 466.0 Å^2) with 72 Ce and 143 O atoms. In both cases, the slabs were separated by a vacuum layer of 20 Å, and the bottom O-Ce-O trilayer was fixed to the bulk lattice during the relaxation. The oxygen vacancy was introduced by removal of one oxygen atom from the top layer of each slab model, which leads to a stoichiometry of $CeO_{1.96}$ and $CeO_{1.99}$ for the small and large surface, respectively. We limited our study to vacancies in the top-layer, although calculations with hybrid functionals predict sub-surface vacancies to be slightly more stable.[57] The reason for this choice is that the clusters can be expected to stabilise top-layer vacancies. Moreover, the influence of sub-surface vacancies on the properties of the supported clusters can be expected to be greater than that of the top-layer vacancies.

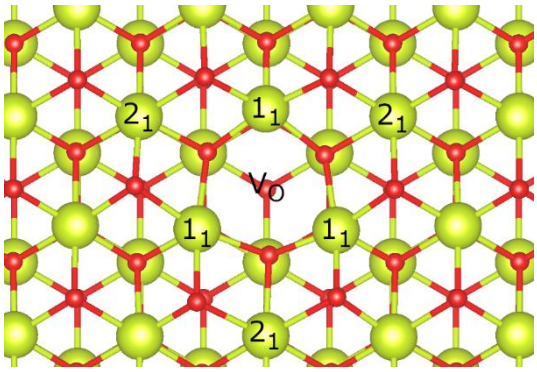

Figure 1: Structure of oxygen-terminated CeO_2(111) with one oxygen vacancy (V_O); the n_m notation is explained in the text; colour scheme: red – O, green – Ce.

The positions of Ce^{3+} ions were directed to the desired configuration by increasing the Ce-O distances at the sites before the optimisation procedure to preferentially accommodate the larger Ce^{3+} ions. To do so, the Ce ion was first replaced by a larger La ion and the structure was optimised. The re-substitution with Ce gave the desired starting structures with increased distances. The positions of the Ce^{3+} ions are labelled according to the distance to the O vacancy (see Figure 1). The notation n_m corresponds to a Ce ion in the n^{th} shell around the defect in the m^{th} cationic layer counted from the surface.[29]

Cluster models

The structures of the supported gold clusters were based on those obtained in our previous study on stoichiometric CeO_2.[24] We chose to investigate structures with 1, 2, 3, 7, 8, 10, and 11 Au atoms, which represent a cross-section through the previously investigated range of cluster sizes including odd- and even-numbered clusters. As we have noted, the structures we generate after adsorption on the surface may not be global minima, but they will still give us the insights needed on the effect of the vacancies on cluster geometry, electronic properties and reactivity.

Results and Discussion

Structures and Binding Energies of supported Au clusters on defective CeO_{2-X}(111)

Based on the structures obtained in our previous study of Au_n clusters on stoichiometric CeO_2, we created O vacancies in different positions. We first discuss the geometric and electronic properties of the structures with the lowest energies and describe the influence of the relative vacancy position in later sections of the text. Further details on the structures can be found in the Supporting Information (Table S 1).

The results of our calculations suggest that the preferred vacancy position and the extent of the influence on the cluster structure are strongly dependent on the cluster size without showing any obvious trend with increasing size within the investigated size range (cf. Table 1). The vacancy is preferentially located centrally under the Au cluster (Au_1, Au_7, Au_8, Au_{11}), under a corner atom of the Au cluster (Au_3, Au_4, Au_{10}), or next to the Au cluster (Au_2). A significant decrease in the cluster-surface distance was found for clusters with 1, 3, 4, and 11 Au atoms compared to the respective clusters on the stoichiometric surface (cf. Table 1). In these cases, the Au atom above the vacancy moves into the vacancy site as shown for Au_4/CeO_{2-X} in Figure 2 (top). The displacement of the Au atom into the vacancy site leads to an elongation of the average Au-Au distances compared to the stoichiometric surface. For Au_4 and Au_{11}, the Au coordination number decreases, since some of the Au-Au distances become longer than the defined threshold (see Computational Details section) so that the elongation is not reflected in the average values shown in Table 1. In other cases, we only observed minor changes in the structural parameters. Interestingly, Au_7 is located centrally on top of the vacancy but no movement of an Au atom into the vacancy site nor was there any other significant structural distortion. (see Figure 2 bottom).

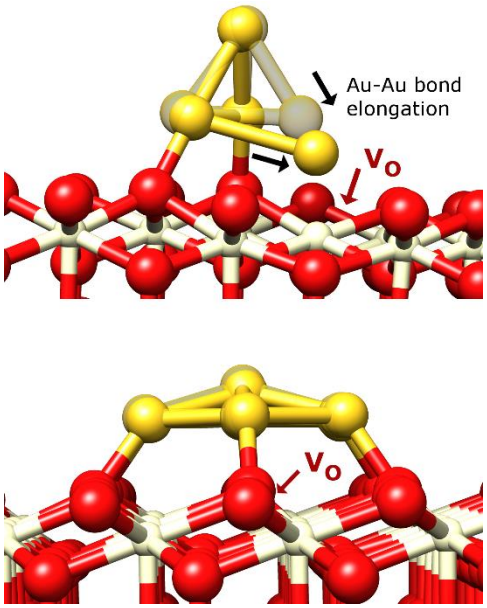

Figure 2: Structure of Au_4 (top) and Au_7 (bottom) on CeO_{2-X} and on CeO_2 (transparent).

The strength of the binding of the Au clusters to the support surface is reflected in the adsorption energies (E_{ads}) shown in Table 1. The values indicate that all clusters except for Au_{10} bind more strongly to the defective CeO_{2-X} surface than to the non-defective CeO_2 surface. The stabilisation of the cluster-surface interaction by the oxygen vacancy (difference in adsorption energy) ranges from −1.79 eV (Au_1) to +0.03 eV (Au_{10}). Interestingly, the cohesion energy of the Au clusters (E_{coh}), which is a measure for the strength of the Au-Au interaction is not significantly decreased for Au_3, Au_4, or Au_{11} although these clusters show the most apparent structural distortion.

Electronic Structure

The underlying reason for the difference in the influence of the oxygen vacancy on the cluster structure can be found in the electronic structure of the investigated systems. The adsorption of Au clusters on stoichiometric CeO_2(111) leads to a charge transfer from the cluster to the surface. The cluster is oxidised while specific Ce^{4+} ions of the CeO_2 lattice are reduced to Ce^{3+}.[24] The number of Ce^{3+} ions depends on the cluster size and whether the cluster has an odd or even number of Au atoms. Odd-numbered clusters are open-shell systems and induce the reduction of an odd number of Ce^{4+} ions while even-numbered clusters are closed shell and result in an even number of Ce^{3+} ions (see Table 1; values in brackets). The magnitude of the charge transfer is approximately proportional to the number of Ce^{3+} ions. Similarly, the introduction of an O vacancy also reduces the surface and creates two Ce^{3+} ions. Since the standard reduction potentials for Au^+ to Au^0 (+1.69 V) and Ce^{4+} to Ce^{3+} (+1.72 V) are very similar,[58] this change in the local environment of the remaining Ce^{4+} ions can change the redox behaviour when an Au cluster is adsorbed.

As shown in Table 1, we found that for the undistorted clusters (Au_2, Au_7, Au_8, and Au_{10}), the number of Ce^{3+} ions in the CeO_{2-X} support is indeed the sum of the number of such ions in the stoichiometric surface with the Au cluster and those from the vacancy formation as if they are not influenced by each other. For these clusters, we calculated approximately the same charge as on the stoichiometric surface. In contrast, we found a lower number of Ce^{3+} ions for Au clusters with 1, 3, 4, and 11 atom(s), which showed a stronger distortion of the cluster structure and smaller cluster-surface distances. In these cases, the number of Ce^{3+} ions equals that found for the stoichiometric surface, which means that there are no additional Ce^{3+} ions due to the O-vacancy. These Au clusters are more electron-rich than non-defective CeO_2. Au_1, Au_3, and Au_4 are indeed reduced by the defective CeO_{2-X} surface, while Au_{11} shows no significant charge transfer with the support surface. The calculated charges are in agreement with previously reported values.[15,19]

The two categories of Au clusters that we identified based on structural parameters and charge transfer also show distinct features in their density of states (DOS). In general, the DOS of stoichiometric CeO_2 shows a bandgap of 2.1 eV between the valence band consisting dominantly of O 2p states and the conduction band dominated by Ce 4f states. If a Au cluster is adsorbed, one singly occupied **k**-independent discreet Ce 4f state of each Ce^{3+} ion can be found at E_F and directly below. With increasing Au cluster size, the number of occupied Au-O bands increases. These bands are occupied by both spins and overlapping the O 2p band or located in the band gap between E_F and the valence band. They show strong Au d- and O p character and increasing Au s character with increasing energy. The DOS of Au_1, Au_3, Au_4, and Au_{11}, which belong to the group of distorted and electron-rich clusters, feature a new type of Au-Ce band with contributions from Au s/d, O p and Ce f orbitals located between the Au-O bands and the occupied Ce 4f states at the Fermi energy. As an example, Figure 3 (top) shows the DOS of Au_3/CeO_{2-X}. Five narrow bands can be found within the bandgap between the O 2p valence band and the Ce 4f conduction band. The first three (**a-c**) show contributions from Au s and d states as well as O p states. Band **d** consists of Au s and d states and Ce f states. At the Fermi energy, a singly occupied Ce 4f state can be found, which is localised at the Ce^{3+} ion. In contrast to this, the DOS of Au_2, Au_7, Au_8, and Au_{10}, which belong to the group of clusters that are not influenced significantly by the vacancy, generally resemble the ones of the same cluster size on the stoichiometric surface with the addition of two more singly occupied Ce 4f peaks close to E_F. These additional Ce f bands are simply a result of the additional two Ce^{3+} ions which are present due to the creation of the oxygen vacancy. In Figure 4 (top), the DOS of Au_7/CeO_{2-X} is shown. Compared to Au_3/CeO_{2-X} (Figure 3 top), the number of states in the O(2p)-Ce(4f) bandgap has increased to nine. Six (**a-f**) can be attributed to Au-O bands and three (**g-i**) to the singly occupied 4f orbitals of the three Ce^{3+} ions.

Table 1: Summary of structural and electronic properties of Au_n cluster on CeO_{2-x}; values in bracket for Au_n/CeO_2; n_{Au}: number of Au atom; d_{Au-Au}: average Au-Au distance;

d_{Au-S}: cluster-surface distance; q_{Au}: total charge of Au_n cluster; E_{ads}: adsorption energy; E_{coh}: cohesion energy; n_{Ce3+}: number of Ce^{3+} ions; * structural distortion leads to change in Au coordination numbers.

n_{Au}	d_{Au-Au} [Å]	d_{Au-S} [Å]	q_{Au} [e]	E_{ads} [eV]	E_{coh} [eV]	n_{Ce3+}	Occ. Au-Ce band
1	n/a	1.27 (1.89)	−0.57 (+0.18)	−3.08 (−1.30)	0.00 (0.00)	1 (1)	Yes
2	2.58 (2.52)	1.69 (1.60)	−0.17 (−0.12)	−3.03 (−1.94)	−1.14 (−1.15)	2 (0)	No
3	2.79 (2.66)	1.20 (2.06)	−0.57 (+0.28)	−4.24 (−3.90)	−1.13 (−1.17)	1 (1)	Yes
4	2.77* (2.76)	1.24 (1.99)	−0.29 (+0.62)	−6.10 (−5.37)	−1.15 (−1.17)	2 (2)	Yes
7	2.74 (2.74)	1.93 (1.98)	+0.16 (+0.20)	−6.45 (−5.75)	−1.83 (−1.82)	3 (1)	No
8	2.76 (2.75)	1.93 (1.98)	+0.39 (+0.53)	−7.69 (−7.28)	−1.68 (−1.77)	4 (2)	No
10	2.83 (2.87)	1.90 (2.03)	+0.38 (+0.52)	−8.19 (−8.22)	−1.94 (−1.94)	4 (2)	No
11	2.89* (2.89)	1.14 (2.04)	+0.07 (+0.81)	−9.72 (−9.43)	−1.93 (−1.90)	3 (3)	Yes

Influence of the Ce^{3+} ion positions

The number of Ce^{3+} ions varies with cluster size and vacancy position, and their localisation can have a significant influence on the total energy of the system.[29] We illustrate here, based on several examples, how different Ce^{3+} positions affect the properties of the system.

If, for example, the Ce^{3+} ion of Au_1/CeO_{2-x} is shifted from the most stable 2_1 position to an 1_1 or 3_1 position, the energy difference between the singly occupied Ce 4f state at E_F and the valence band is increased by 0.44 eV and 0.15 eV, respectively. However, the bandgap between the O 2p valence band and Ce 4f conduction band (2.1 eV) as well as the general shape of the DOS (see Figures S3 and S4 in the Supporting Information) remains unaffected. Therefore, it can be concluded that the increase in the total energy compared to the localisation in 2_1 position of these systems is caused by the occupation of a Ce 4f state with higher energy, meaning that the occupation of this state has negligible influence on other states and the properties of the adatom. The charge transfer between the surface and the Au atom with Ce^{3+} in 1_1 position is −0.60 e, only 0.03 e different from the 2_1 position. Similarly, the positions of the two Ce^{3+} ions of Au_2/CeO_{2-x} only have an influence on the total energy of the system, i.e. with one (2_1-1_1) or both Ce^{3+} ions located directly next to the vacancy (1_1-1_1), the energy is +0.05 eV and +0.13 eV higher, respectively, which, however, has only a minor effect on the charge transfer (–0.18 and –0.20 e). The same was observed, for example, for Au_7/CeO_{2-x}, which features three Ce^{3+} ions. Their arrangement in 1_1-2_1-2_1 positions, i.e. under (1_1) and next to the cluster (2_1), is favoured over a 2_1-2_1-2_1 arrangement with all Ce^{3+} ions next to the cluster. However, the energy difference is merely 0.04 eV. The Au cluster has a positive charge of +0.16 e in the former and +0.12 e in the latter case.

These examples show, that in most cases, there is only a minor influence of the position of the Ce^{3+} ions on the electronic structure of the Au clusters and their charge, suggesting that the implications of the Ce^{3+} ion positions on the herein investigated cluster properties are in general very low, although there could be configurations not explored here where it could be more significant

We should also note a significant observation for Au_{10}/CeO_{2-X}. The lowest energy structure has four Ce^{3+} ions in 1_1-1_1-1_1-3_1 positions. In an attempt to localise three of them next to the corners of the Au_{10} cluster, we obtained a final structure with only two Ce^{3+} ions, one at a 1_1 position next to the vacancy (under the centre of the cluster) and the second one at a 3_1 position next to one of the corners of the cluster. The Au atom above the oxygen vacancy is lowered into the vacancy site and a strong change in the charge transfer can be observed. While the Au cluster was oxidised in the lowest energy structure with a charge of +0.38 e, it is reduced in the structure with only two Ce^{3+} ions with a charge of −0.35 e. While this newly obtained structure with a reduced Au cluster is higher in energy by 0.24 eV, it shows that there can be multiple minima with the same vacancy location, but a different number of Ce^{3+} ions resulting in significant structural and electronic changes at the cluster.

Furthermore, it should be considered that our localisation method using a structural distortion (see Methods section) can only loosely direct the optimisation procedure to a certain localisation pattern meaning. Moreover, in a dynamic system, the vibrations of the support lattice will create temporary distortions of the structure around the Ce ions. These distortions will shift the 4f electron density between these ions in the same way as our intentional distortions to direct the Ce^{3+} ion positions.[59] Inclusion of dynamic effects would be an interesting future study for this system.

Journal Name

ARTICLE

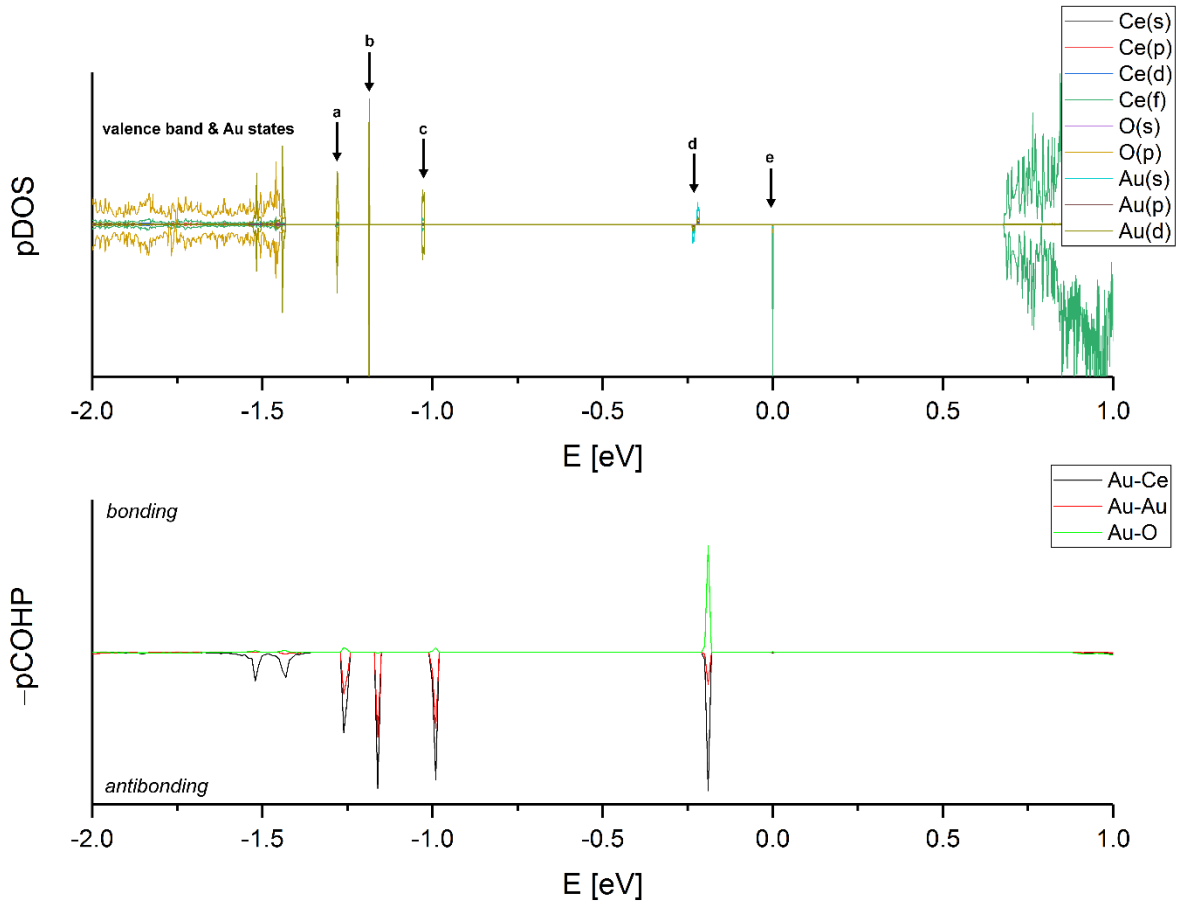

Figure 3: DOS (top) and COHP (bottom) of Au_3/CeO_{2-x}; average COHP of all respective pairs with a maximum distance of 4.0 Å; energies relative to E_F.

Influence of the vacancy position

In general, the position of the oxygen vacancy relative to an Au cluster has a more significant influence on the cluster properties than the Ce^{3+} ion positions (cf. Table 2). For the first group of clusters (Au_1, Au_3, Au_4, Au_{11}), which are more electron-rich than the respective clusters on the stoichiometric surface, the vacancy is initially located underneath the cluster. Moving it to a position outside the cluster perimeter results in an increase of the number of Ce^{3+} ions to the sum of the number of ions in Au_n/CeO_2 and the two Ce^{3+} ions in a naked defective CeO_{2-x} surface. The Au-Ce band disappears from the DOS and the charge transfer is similar to the stoichiometric surface. For any vacancy position outside the cluster perimeter, we did not find an influence of the exact position of the vacancy relative to the cluster on the investigated properties. For example, for Au_3/CeO_{2-x}, we calculated two structures with different vacancy positions next to the cluster (Table 2; entries 5 and 6; see Figure S1 in the Supporting Information for details). Both structures are only higher in energy by 0.01 eV with respect to the one with the vacancy right below the cluster. In both cases, the oxygen vacancy has no significant influence on the structure and charge of the trimer compared to the stoichiometric surface. In the case of Au_{11}, the vacancy can also be positioned under a corner atom instead of under the centre of the cluster, which leads to a lower cluster charge of −0.09 e compared to +0.07 e before.

For Au_8 and Au_{10}, which belong to the second group of clusters and are initially unaffected by the oxygen vacancy, we found that their behaviour is similar to the first group when the vacancy is placed underneath a corner atom of the cluster. In both cases (Au_8 and Au_{10}), the Au cluster is structurally distorted and more electron-rich than on stoichiometric CeO_2, the number of Ce^{3+} ions is decreased, and the DOS shows an occupied Au-Ce band. For example, if the oxygen vacancy is located underneath a Au atom of the Au_8 cluster underneath

the second layer Au atom, this atom moves into the oxygen vacancy site (Table 2; entry 12; Table S1 in Supporting Information). The average Au-Au distance is decreased from 1.93 to 1.21 Å, and the cluster-surface distance is increased from 2.76 to 2.81 Å. The Au cluster is reduced with a charge of −0.34 e instead of being oxidised with a charge of +0.39 e. Moreover, two instead of four Ce^{3+} ions can be found in the surface and the DOS shows occupied Au-Ce bands. We removed the oxygen atom underneath the lower atom of Au_2 on CeO_{2-x} to create an oxygen vacancy at that position, but the structure relaxed during the geometry optimisation procedure to one equivalent to the one described previously.

Table 2: Summary of structural and electronic properties of Au_n cluster on CeO_{2-x} with varied vacancy positions; values in bracket for Au_n/CeO_2; n_{Au}: number of Au atom; d_{Au-Au}: average Au-Au distance; d_{Au-S}: cluster-surface distance; q_{Au}: total charge of Au_n cluster; n_{Ce3+}: number of Ce^{3+} ions; * structural distortion leads to change in Au coordination numbers; see Table S1 in the Supporting Information for details on the structures.

Entry	n_{Au}	V_O position	d_{Au-Au} [Å]	d_{Au-S} [Å]	q_{Au} [e]	n_{Ce3+}	Occ. Au-Ce band
1	1	corner	n/a	1.27 (1.89)	−0.57 (+0.18)	1 (1)	Yes
2	1	next	n/a	1.70 (1.89)	−0.16 (+0.18)	2 (1)	No
3	2	next	2.58 (2.52)	1.60 (1.69)	−0.17 (−0.12)	2 (0)	No
4	3	corner	2.79 (2.66)	1.20 (2.06)	−0.57 (+0.28)	1 (1)	Yes
5	3	next	2.66	2.07	+0.24 (+0.28)	3 (1)	No
6	3	next	2.66	2.08	+0.25 (+0.28)	3 (1)	No
7	4	corner	2.77*(2.76)	1.24 (1.99)	−0.29 (+0.62)	2 (2)	Yes
8	4	next	2.76 (2.76)	1.98 (1.99)	+0.56 (+0.62)	4 (2)	No
9	7	centre	2.74 (2.74)	1.93 (1.98)	+0.16 (+0.20)	3 (1)	No
10	7	corner	2.77 (2.74)	1.94 (1.98)	+0.05 (+0.20)	3 (1)	No
11	8	centre	2.76 (2.75)	1.93 (1.98)	+0.39 (+0.53)	4 (2)	No
12	8	corner	2.81 (2.75)	1.21 (1.98)	-0.34 (+0.53)	2 (2)	Yes
13	8	next	2.75 (2.75)	1.99 (1.98)	+0.50 (+0.53)	4 (2)	No
14	10	edge	2.83 (2.87)	1.90 (2.03)	+0.38 (+0.52)	4 (2)	No
15	10	corner	2.85* (2.87)	1.25 (2.03)	-0.39 (+0.52)	2 (2)	Yes
16	10	next	2.87 (2.87)	2.02 (2.03)	+0.49 (+0.52)	4 (2)	No
17	11	centre	2.89* (2.89)	1.14 (2.04)	+0.07 (+0.81)	3 (3)	Yes
18	11	corner	2.83 (2.89)	1.37 (2.04)	-0.09 (+0.81)	3 (3)	Yes
19	11	next	2.87 (2.89)	2.03 (2.04)	+0.86 (+0.81)	5 (3)	No

As the results show, the charge of the Au particle is highly dependent on the vacancy position. However, it is essential to consider whether this affects all cluster atoms or if it is a local effect to those atoms directly at the vacancy. Table 3 shows the variation in the calculated atomic charges for Au_8/CeO_{2-x} with different vacancy positions relative to the cluster on the stoichiometric surface. When the vacancy site is beneath the central Au atom (a), the charge difference at the central Au atom of the cluster (Au atom 1) contributes 50 % of the total charge difference of the cluster (Δq = −0.07 e). The total cluster charge changes most (Δq = −0.88 e) if the vacancy is located under the corner Au atom under the second layer Au atom (b). Our results suggest that the atom at the vacancy site (Au atom 2) contributes with −0.74 e, more than seven times more than the next most influenced atom (Au atom 3; −0.09 e), which is located next to the vacancy. The impact of an oxygen vacancy next to the cluster (c) on the cluster charge is negligible (−0.03 e) which is reflected in the minor charge differences of each Au atom. In Au_{11}/CeO_{2-x}, the oxygen vacancy is located centrally under the Au_{11} cluster. Compared to the stoichiometric surface, the total charge of the cluster decreases from +0.81 e to +0.07 e. The charges at each Au atom show that none of the atoms at the cluster interface is affected by more than ±0.03 e. The only significant charge difference can be found for the Au atom at the vacancy with −0.65 e compared to the stoichiometric surface. This local character of the influence of the oxygen vacancy on the charge of the Au atoms has implications for the catalytic activity of the Au particles. The Au atoms at the vacancy, which are almost exclusively affected by the vacancy, are in many cases less or not at all accessible for any substrate. Hence, according to the atomic charge distribution, the reactivity of the catalytically active atoms at the cluster surface remain practically unaffected.

Table 3: Changes of Bader charges of Au atoms in Au_8/CeO_{2-x} compared with Au_8/CeO_2; vacancy located under central Au atom (a), corner Au atom (b), and next to the cluster (c).

Au atom	q [eV] (a)	q [eV] (b)	q [eV] (c)
1	−0.07	+0.02	0.00
2	0.00	−0.74	−0.03
3	0.00	−0.09	+0.01
4	−0.02	+0.02	0.00
5	−0.01	−0.02	+0.03
6	0.00	−0.06	−0.01
7	−0.02	+0.02	0.00
8	−0.01	−0.03	−0.01
SUM	−0.14	−0.88	−0.03

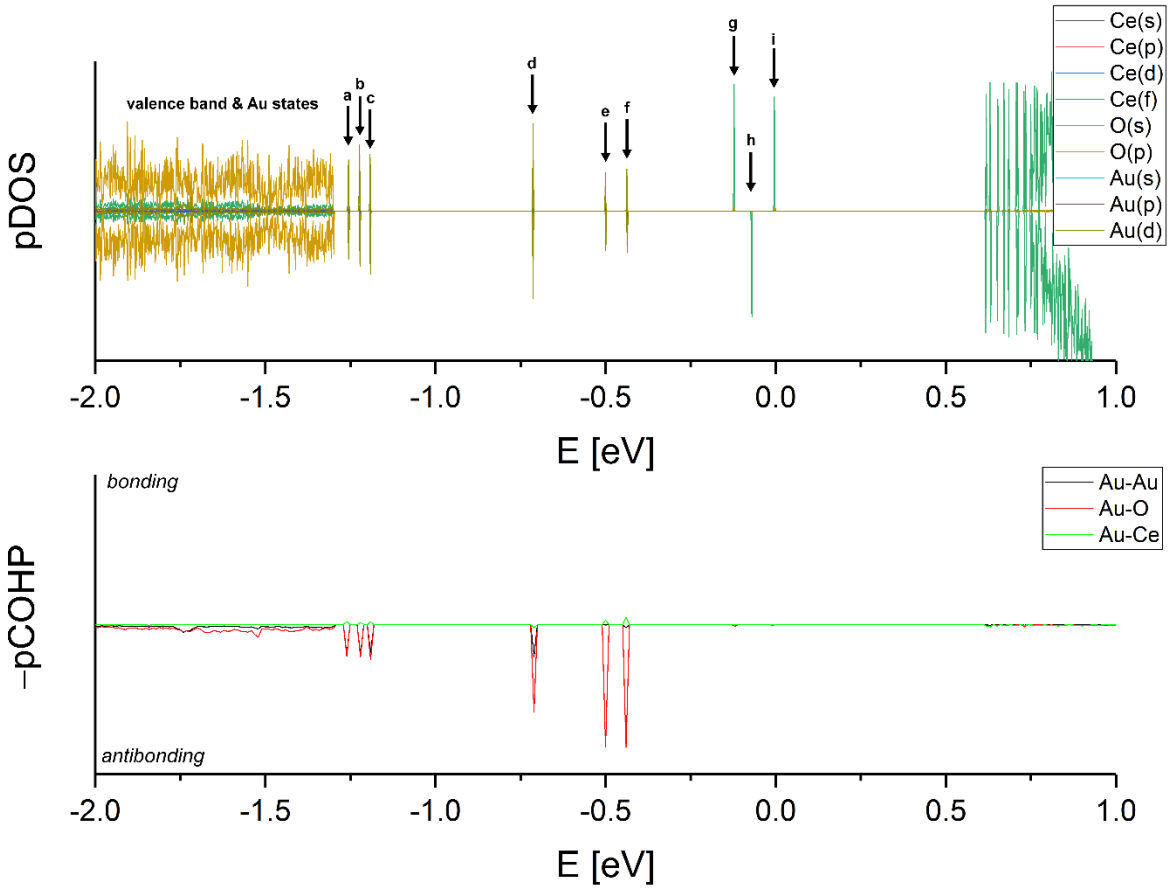

Figure 4: DOS (top) and COHP (bottom) plot of Au_7/CeO_{2-x}; average COHP of all respective pairs with a maximum distance of 4.0 Å.

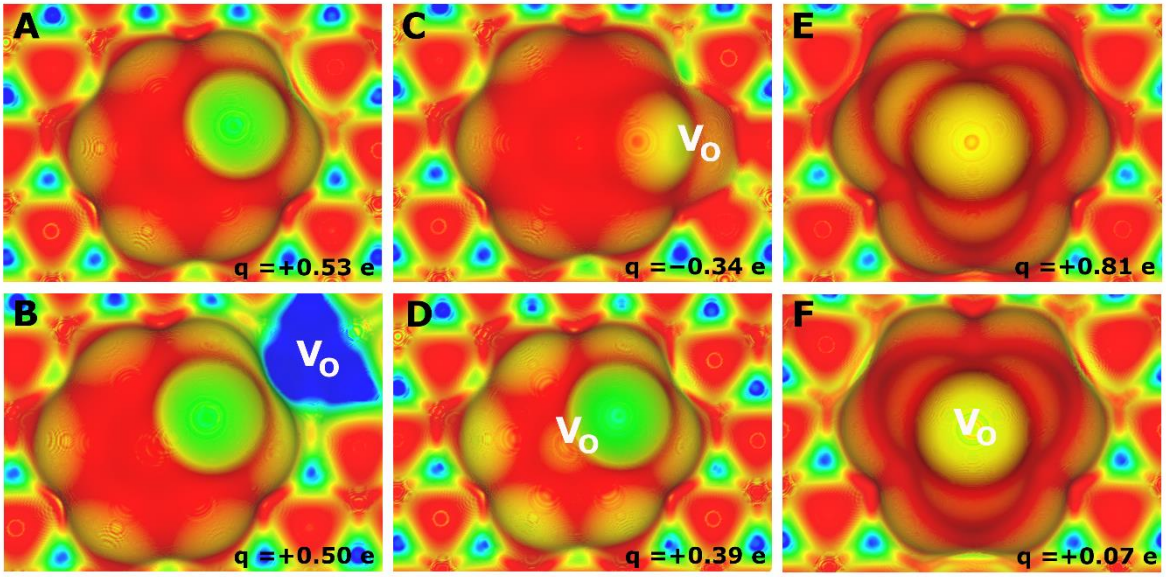

Figure 5: Iso-surfaces of the electron density (iso-value: 0.001 a.u) mapped with the (electrostatic) local potential; colour scale between ≥0 eV (blue) and ≤−2.5 eV (red); V_O: oxygen vacancy position; q: charge of Au_n cluster; A: Au_8/CeO_2; B: Au_8/CeO_{2-x} with vacancy next to cluster; C: Au_8/CeO_{2-x} with vacancy under corner atom; D: Au_8/CeO_{2-x} with vacancy under central cluster atom; E: Au_{11}/CeO_2; F: Au_{11}/CeO_{2-x} with vacancy under central atom.

The Bader charge analysis allows us to designate charges to single atoms but does not account for the spatial distribution of the charge density around the respective atoms. We used the electrostatic potential to identify sites with low electron

density, which can indicate potential (electrostatic) interaction sites of the cluster with other molecules.[54,60–64] Figure 5 shows the electrostatic potential mapped on the 0.001 au electron density iso-surfaces of the three different Au_8 structures on the defective and stoichiometric surface. The chosen iso-value was used in previous studies and approximately corresponds to the van-der-Waals surface of the molecules.[60,63] In all four images, σ-holes are visible at each corner atom as well as the Au atom of the second layer in agreement with previous reports.[60,63] The σ-holes at the corner atoms are most pronounced when the oxygen vacancy is located centrally under the cluster (Figure 5 D) and least visible when the vacancy is located under one of the corner Au atoms (Figure 5 C). The images of Au_8 on the stoichiometric surface (Figure 5 A) and with the vacancy next to the cluster (Figure 5 B) show no distinct differences. However, the decrease of the magnitude of the σ-holes cannot be directly correlated to the charge of the Au clusters as the vacancy only affects the charge of the gold atoms directly at the vacancy. Nevertheless, there is an indirect influence of the vacancy on the distribution of the electron density. We performed single-point calculations of isolated Au_8 clusters with the same geometry as the ones on CeO_{2-x} (see Table S2 in the Supporting Information). The results show that even in the absence of any surface, the σ-holes are more visible in the structure where the vacancy was located under the Au cluster compared to the one where the vacancy was located outside the cluster perimeter. The vacancy induces a small structural change, namely the movement of the central atom of the first Au layer, increasing the planarity of the first layer of Au atoms. The increased planarity enhances the overlap between the Au atoms while decreasing the electron density on the adjacent position of the Au atoms. Comparison of the electrostatic potentials of Au_{11} on stoichiometric CeO_2 (Figure 5 E) and defective CeO_{2-x} (Figure 5 F), shows that the oxygen vacancy amplifies the σ-hole at the top of the cluster under the cluster. However, the regions with low electron density at the corners of the second layer of Au atoms decreases. As in the case of Au_8, both differences can also be found for clusters of these shapes without the support surface (see Tables S3 and S4 in the Supporting Information) suggesting that they are a result of the structural change induced by the oxygen vacancy (lower central Au atom of the first layer) rather than an effect of the charge transfer between the surface and the cluster. The σ-holes at the Au atoms of the second layer are formed due to interactions with the central atom of the first layer. Since this atom moves into the vacancy, the overlap between those atoms and, consequently, the magnitude of the σ-hole decreases. The more subtle change to the σ-hole at the top of the cluster can be rationalised by a contraction of the atoms in the lower layers, which concentrates the area of low electron density at the top of the cluster to a smaller area but increases its magnitude.

These results show that the position of the vacancy relative to the cluster influences the structure but also on the electronic structure of the clusters. Depending on the position of the vacancy, the clusters can be assigned to one of the two categories: (i)those showing distortion of the cluster geometry, usually one Au atom in the vacancy site, together with a lower total charge, lower number of Ce^{3+} ions and formation of a Au-Ce band and (ii) those in which neither their geometry nor electronic structure is significantly affected by the vacancy. In general, it can be said that if the vacancy is not located under one of the Au atoms, it does not affect the cluster properties. However, it is less obvious to derive a rule for the different positions under an Au cluster since the specific properties of the cluster play an important role.

Rationalisation of the charge transfer/Formation of Au-Ce bonds

To better understand why some clusters exhibit a substantial change in their properties due to the vacancy, we used Crystal Orbital Hamilton Population (COHP) and analysed the electronic structure of the supported clusters. COHP is a powerful tool to distinguish whether states or regions of the DOS are contributing to the stabilisation of the structure, or are destabilising it.[49]

The COHP of Au_3/CeO_{2-X} is depicted in Figure 3, together with the respective DOS. The COHP is evaluated for Au-Au, Au-O and Ce-O pairs to cover all relevant interactions. The plot shows that the Au-O bands (**a-c**) have antibonding character within the cluster between the Au atoms as well as between the Au atoms of the cluster and the surface O atoms. Note that, the occupied Ce 4f band **e** is not visible in the COHP due to its non-bonding nature. The Au-Ce band (d) is formed by the interaction of a Ce^{3+} ion with the singly occupied s-dominated Au orbital resulting in increased electron density at the Au cluster, more precisely at the Au atom at the vacancy site. The COHP indicates that this band is strongly antibonding concerning the Au-Au interactions, which means that it leads to a destabilisation of the Au cluster. This is reflected in the previously described elongation of the average Au-Au distances. The iso-surface of this band shows the strong s character at the Au atom in the vacancy site (see Figure S16 in the Supporting Information). The same observations can be made for all clusters of the first group (Au_1, Au_3, Au_4, Au_{11}). The respective DOS/COHP plots can be found in the Supporting Information.

The stabilising effect for Au atoms at the vacancy site was described previously and attributed to the pairing of the Au s electrons as well as ionic interaction between the Au and Ce atoms.[15] The fact that the DOS (see Figure S2 in the Supporting Information) shows a shared bonding Au-Ce orbital with significant contribution by Ce 4f states can be seen as evidence for some degree of the covalent character of the Au-Ce interaction.

The clusters of the second group do not show such Au-Ce interaction although in some cases (Au_7, Au_8), the vacancy is preferentially located centrally under the cluster. The COHP of Au_7/CeO_{2-X} shows indeed no significant deviation of the Au-Ce plot from zero (see Figure 4). The Au-O bands (**a-f**) are antibonding with respect to the Au-Au and Au-O pairs, and the Ce 4f bands (**g-i**) are non-bonding. The presence of an additional Ce^{3+} ion in the surface compared to the naked defective CeO_{2-X} surface indicates that electron density is shifted from occupied antibonding Au-O states into one of the non-bonding Ce 4f states. The reason for the absence of an Au-Ce bond can be found in the geometry of the Au_7 cluster. The central Au atom

is farther away from the surface than all other Au atoms, which indicates that a weak interaction.

We artificially distorted the structure of the Au_7 cluster by moving the central atom into the vacancy site, but this structure was found to be unstable and reverted during the geometry optimisation process. It was discussed previously that the Au atoms at the vacancy move upward for clusters larger than four Au atoms due to strong Au-Au interactions.[19] Our results show a more detailed explanation, i.e. the formation of Au-Ce bonds destabilises the Au-Au bonds within the cluster. However, the Au-Au interactions at the central atom are particularly crucial for the stability of the Au_7 cluster. Its coordination number is higher than any other Au atom in the cluster and it is connected to every other Au atom of the cluster. Due to the increased distance to the vacancy, there is no charge transfer from the Ce^{3+} ions into antibonding Au-Au bands. The O-Au(corner)-Au(central) angle is significantly decreased if the central Au atom moves into the vacancy, which would decrease the overlap between the orbitals of the corner atoms of the cluster and those of the surface oxygen atoms. If the vacancy is located under one of the corner atoms, the rigidity of the planar Au_7 structure disfavours the formation of an Au-Ce bond. The reduced charge transfer compared to the vacancy location under the central Au atom can simply be explained by the loss of one of the Au-O bonds. Au_8 is structurally more flexible than Au_7.

The COHP of Au_8/CeO_{2-x} with the vacancy located under the central Au atom of the first layer shows one band with low bonding character between Au and Ce (see Figure S7 in the Supporting Information). This band has mainly contributions from Au(d) and O(p) states but also a low amount of Ce(f) character. This interaction with the Ce^{3+} ions under the cluster can explain the reduced charge transfer (+0.39 e) compared to the stoichiometric surface (+0.53 e). Our calculations show that, in contrast to Au_7, a vacancy under one of the corner atoms of Au_8 can lead to a distortion of the cluster and the formation of Au-Ce bands. The atom above the vacancy moves into the vacancy site and the Au atom of the second layer takes its place in the Au_7 layer (see Table S1 in the Supporting Information). The DOS shows three bands with Au and Ce contributions in the investigated energy range (see Figure S8 in the Supporting Information). According to the COHP, all three bands are bonding with respect to Au-Ce pairs. The iso-surface of the most bonding band between Au and Ce shows significant s character at the Au atom in the vacancy site (see Figure S22 in the Supporting Information).

The DOS of Au_{10}/CeO_{2-x} shows no occupied Au-Ce bands in the energy range considered when the vacancy is located under the cluster edge (see Figure S9 in the Supporting Information). However, there is an unoccupied Au-Ce band with strong bonding character only 0.16 eV above E_F with strong Au(s), Au(d), and Ce(f) contribution, meaning that there is a small energy gap to occupy this band and form an Au-Ce bond, which explains why we found a structural change when relocating the Ce^{3+} ions.

For Au_{11}, we found an Au-Ce band (**g**) with strong Au(s) and Ce(f) character located 0.08 eV below E_F (see Figure S10 in the Supporting Information). This band shows strong bonding properties between Au and Ce atoms in the COHP Thus, the difference between Au_7 to Au_{11}, which have the same hexagonal structure at the cluster-surface interface, is that the central atom of the first Au layer moves into the vacancy position, which allows for a significant orbital overlap between the Au(s) states and the Ce(f) states. Such a deformation did not occur for Au_7 due to the strong destabilisation of the cluster structure and the rigidity of the planar Au_7 structure. The three-dimensional structure of Au_{11} decreases the relative importance of the Au-Au interactions of the central Au atom of the first layer for the overall cluster stability. Furthermore, the atom from the second Au layer is located in a position to form an O(surface)-Au(corner)-Au(2^{nd} layer) angle of 170° at all corners, which allows stronger Au-O interactions as in the case of the distorted Au_7 structure.

This analysis shows that the oxygen vacancies can lead to increased electron density at the Au clusters by the formation of an Au-Ce bond. The Au-Ce bonds have strong s-character at the Au atom in the vacancy site. Electron density is shifted from one of the Ce^{3+} ions into the newly formed orbital, which explains the lower (or more negative) charge at the Au cluster but also the local character of the effect. However, this interaction destabilises the Au-Au and Au-O interactions, which is reflected in the structural distortion of these clusters. Whether a cluster of a specific size is affected by the oxygen vacancy is ultimately decided by the rigidity of the cluster structure or the importance of the interactions of the Au atom at the vacancy with the rest of the cluster. Both the rigidity and the importance of single Au-Au interactions decrease with increasing cluster size so that it can be expected that they will tend to fall into the first category. At the same time, the effect of the vacancy on the exposed cluster interface decreases with increasing size so that the influence on the reactivity can be expected to decrease.

Summary and Conclusions

Our DFT-D(+U) study on the influence of oxygen vacancies in CeO_{2-X} on supported Au clusters shows that there are, in general, two groups of clusters. The first is strongly affected by the presence of an oxygen vacancy, as reflected in their structural distortion, lower cluster charge, and the formation of an Au-Ce bond. The second shows the same properties as on the stoichiometric CeO_2 surface. The decisive parameters are the rigidity of the Au cluster and the importance of the Au-Au bonds for the overall stability of the cluster, which decrease with increasing cluster size.

We also found that the increased electron density at the Au cluster is a local effect and limited to the Au atom at the vacancy site. Investigation of electrostatic potential maps shows that any change of the electron density at the exposed cluster surface can be attributed exclusively to structural changes without any effect of the additional electron density at the Au atom at the vacancy.

Our calculations show that, while the position of the Ce^{3+} ions has a significant influence on the total energy of the system,

other properties such as structure or charge transfer are surprisingly unchanged. These properties can change significantly if a vacancy is underneath a cluster or next to it and the search for the vacancy position with the lowest energy increases the search space regarding the Ce^{3+} positions for each successive displacement of the vacancy site from the cluster. These factors will play an important role in influencing the reactivity of the clusters.

Conflicts of interest

There are no conflicts to declare.

Acknowledgements

UK Catalysis Hub is thanked for resources and support provided through our membership of the UK Catalysis Hub Consortium and funded by the Engineering and Physical Sciences Research Council (EPSRC) (grants EP/K014706/1, EP/K014668/1, EP/K014854/1, EP/K014714/1, and EP/M013219/1). We also thank the EPSRC for the support through the EP/P005845/1 grant. Via our membership of the UK's HEC Materials Chemistry Consortium, which is funded by EPSRC (EP/L000202), this work used the UK Materials and Molecular Modelling Hub for computational resources, MMM Hub, which is partially funded by EPSRC (EP/P020194). We also acknowledge computing time on the facilities of Supercomputing Wales and the Advanced Research Computing @ Cardiff (ARCCA) at Cardiff University.

Notes and references

1 Q. Fu, A. Weber and M. Flytzani-Stephanopoulos, *Catal. Lett.*, 2001, **77**, 87–95.
2 X. Zhao, L. Wei, S. Cheng and J. Julson, *Catalysts*, 2017, **7**, 83–107.
3 R. Schlögl, *Angew. Chemie Int. Ed.*, 2015, **54**, 3465–3520.
4 G. J. Hutchings, *J. Catal.*, 1985, **96**, 292–295.
5 M. Haruta, *Gold Bull.*, 2004, **37**, 27–36.
6 M. D. Hughes, Y. J. Xu, P. Jenkins, P. McMorn, P. Landon, D. I. Enache, A. F. Carley, G. A. Attard, G. J. Hutchings, F. King, E. H. Stitt, P. Johnston, K. Griffin and C. J. Kiely, *Nature*, 2005, **437**, 1132–1135.
7 P. Liu, J. Hrbek, J. Evans and M. Pérez, *Angew. Chemie*.
8 A. Corma and H. Garcia, *Chem. Soc. Rev.*, 2008, **37**, 2096.
9 X. Zhou, W. Xu, G. Liu, D. Panda and P. Chen, *J. Am. Chem. Soc.*, 2010, **132**, 138–146.
10 M. M. Schubert, A. Venugopal, M. J. Kahlich, V. Plzak and R. J. Behm, *J. Catal.*, 2004, **222**, 32–40.
11 B. Hvolbæk, T. V. W. Janssens, B. S. Clausen, H. Falsig, C. H. Christensen and J. K. Nørskov, *Nano Today*, 2007, **2**, 14–18.
12 N. Lopez, T. V. W. Janssens, B. S. Clausen, Y. Xu, M. Mavrikakis, T. Bligaard and J. K. Nørskov, *J. Catal.*, 2004, **223**, 232–235.
13 M. Cargnello, V. V. T. Doan-Nguyen, T. R. Gordon, R. E. Diaz, E. A. Stach, R. J. Gorte, P. Fornasiero and C. B. Murray, *Science (80-.).*, 2013, **341**, 771–773.
14 Z.-P. Liu, S. J. Jenkins and D. A. King, *Phys. Rev. Lett.*, 2005, **94**, 196102.
15 C. Zhang, A. Michaelides, D. A. King and S. J. Jenkins, *J. Chem. Phys.*, 2008, **129**, 194708.
16 M. F. Camellone and S. Fabris, *J. Am. Chem. Soc.*, 2009, **131**, 10473–10483.
17 N. C. Hernández, R. Grau-Crespo, N. H. de Leeuw and J. F. Sanz, *Phys. Chem. Chem. Phys.*, 2009, **11**, 5246.
18 A. Chutia, D. J. Willock and C. R. A. Catlow, *Faraday Discuss.*, 2018, **208**, 123–145.
19 C. Zhang, A. Michaelides, D. A. King and S. J. Jenkins, *J. Am. Chem. Soc.*, 2010, **132**, 2175–2182.
20 B.-T. Teng, F.-M. Wu, W.-X. Huang, X.-D. Wen, L.-H. Zhao and M.-F. Luo, *ChemPhysChem*, 2012, **13**, 1261–1271.
21 R. Van Den Berg, G. Prieto, G. Korpershoek, L. I. Van Der Wal, A. J. Van Bunningen, S. Lægsgaard-Jørgensen, P. E. De Jongh and K. P. De Jong, *Nat. Commun.*, 2016, **7**, 20457–20465.
22 J. C. Frost, *Nature*, 1988, **334**, 577–580.
23 L. Liu and A. Corma, *Chem. Rev.*, 2018, **118**, 4981–5079.
24 J. Engel, S. Francis and A. Roldan, *Phys. Chem. Chem. Phys.*, 2019, **21**, 19011–19025.
25 G. W. Watson, E. T. Kelsey, N. H. De Leeuw, D. J. Harris and S. C. Parker, *J. Chem. Soc. - Faraday Trans.*, 1996, **92**, 433–438.
26 C. R. Henry, *Henry~Surface Sci. Reports*, 1998, **31**, 231–325.
27 D. R. Mullins, *Surf. Sci. Rep.*, 2015, **70**, 42–85.
28 J. A. Rodriguez, X. Wang, P. Liu, W. Wen, J. C. Hanson, J. Hrbek, M. Pérez and J. Evans, *Top. Catal.*, 2007, **44**, 73–81.
29 J. Paier, C. Penschke and J. Sauer, *Chem. Rev.*, 2013, **113**, 3949–3985.
30 G. Kresse and J. Hafner, *Phys. Rev. B*, 1993, **47**, 558–561.
31 G. Kresse and J. Furthmüller, *Phys. Rev. B*, 1996, **54**, 11169–11186.
32 G. Kresse and D. Joubert, *Phys. Rev. B*, 1999, **59**, 1758–1775.
33 J. Perdew, K. Burke and M. Ernzerhof, *Phys. Rev. Lett.*, 1996, **77**, 3865–3868.
34 R. M. Olson, S. Varganov, M. S. Gordon, H. Metiu, S. Chretien, P. Piecuch, K. Kowalski, S. A. Kucharski and M. Musial, *J. Am. Chem. Soc.*, 2005, **127**, 1049–1052.
35 A. R. Puigdollers, P. Schlexer and G. Pacchioni, *J. Phys. Chem. C*, 2015, **119**, 15381–15389.
36 S. Grimme, J. Antony, S. Ehrlich and H. Krieg, *J. Chem. Phys.*, 2010, **132**, 154104.
37 P. E. Blöchl, *Phys. Rev. B*, 1994, **50**, 17953–17979.
38 H. Monkhorst and J. Pack, *Phys. Rev. B*, 1976, **13**, 5188–5192.
39 J. Hubbard, *Proc. R. Soc. Lond. A. Math. Phys. Sci.*, 1963, **276**, 238–257.
40 J. Hubbard, *Proc. R. Soc. A Math. Phys. Eng. Sci.*, 1964, **277**, 237–259.
41 J. Hubbard, *Proc. R. Soc. A Math. Phys. Eng. Sci.*, 1964, **281**, 401–419.
42 J. Hubbard, *Proc. R. Soc. A Math. Phys. Eng. Sci.*, 1965, **285**, 542–560.
43 J. Hubbard, *Proc. R. Soc. A Math. Phys. Eng. Sci.*, 1967, **296**,

82–99.
44 J. Hubbard, *Proc. R. Soc. A Math. Phys. Eng. Sci.*, 1967, **296**, 100–112.
45 A. I. Liechtenstein, V. I. Anisimov and J. Zaanen, *Phys. Rev. B*, 1995, **52**, R5467–R5470.
46 A. Bruix, J. A. Rodriguez, P. J. Ramírez, S. D. Senanayake, J. Evans, J. B. Park, D. Stacchiola, P. Liu, J. Hrbek and F. Illas, *J. Am. Chem. Soc.*, 2012, **134**, 8968–8974.
47 C. Loschen, J. Carrasco, K. M. Neyman and F. Illas, *Phys. Rev. B - Condens. Matter Mater. Phys.*, 2007, **75**, 035115.
48 W. Tang, E. Sanville and G. Henkelman, *J. Phys. Condens. Matter*, 2009, **21**, 084204.
49 R. Dronskowski and P. E. Blöchl, *J. Phys. Chem.*, 1993, **97**, 8617–8624.
50 V. L. Deringer, A. L. Tchougréeff and R. Dronskowski, *J. Phys. Chem. A*, 2011, **115**, 5461–5466.
51 S. Maintz, V. L. Deringer, A. L. Tchougréeff and R. Dronskowski, *J. Comput. Chem.*, 2013, **34**, 2557–2567.
52 S. Maintz, V. L. Deringer, A. L. Tchougréeff and R. Dronskowski, *J. Comput. Chem.*, 2016, **37**, 1030–1035.
53 A. Bondi, *J. Phys. Chem. A*, 1964, **68**, 441–451.
54 J. S. Murray and P. Politzer, *Wiley Interdiscip. Rev. Comput. Mol. Sci.*, 2011, **1**, 153–163.
55 K. Momma and F. Izumi, *J. Appl. Crystallogr.*, 2011, **44**, 1272–1276.
56 E. F. Pettersen, T. D. Goddard, C. C. Huang, G. S. Couch, D. M. Greenblatt, E. C. Meng and T. E. Ferrin, *J. Comput. Chem.*, 2004, **25**, 1605–1612.
57 M. V. Ganduglia-Pirovano, J. L. F. Da Silva and J. Sauer, *Phys. Rev. Lett.*, , DOI:10.1103/PhysRevLett.102.026101.
58 P. Vanýsek, in *CRC Handbook of Chemistry and Physics: a ready-reference book of chemical and physical data*, ed. W. M. Haynes, CRC Press, 92nd edn., 2011.
59 N. Daelman, M. Capdevila-Cortada and N. López, *Nat. Mater.*, 2019, **18**, 1215–1221.
60 J. H. Stenlid and T. Brinck, *J. Am. Chem. Soc.*, 2017, **139**, 11012–11015.
61 J. S. Murray, P. Lane and P. Politzer, *J. Mol. Model.*, 2009, **15**, 723–729.
62 T. Clark, M. Hennemann, J. S. Murray and P. Politzer, *J. Mol. Model.*, 2007, **13**, 291–296.
63 J. Halldin Stenlid, A. J. Johansson and T. Brinck, *Phys. Chem. Chem. Phys.*, 2019, **21**, 17001–17009.
64 F. A. Bulat, A. Toro-Labbé, T. Brinck, J. S. Murray and P. Politzer, *J. Mol. Model.*, 2010, **16**, 1679–1691.

